Intermetallics 18 (2010) 2343–2352

Contents lists available at ScienceDirect

Intermetallics

journal homepage: www.elsevier.com/locate/intermet

Semi-grand canonical Monte Carlo simulation of ternary bcc lattice-gas decomposition: Vacancy formation correlated with B2 atomic ordering in A–B intermetallics

A. Biborski [a,*], L. Zosiak [a], R. Kozubski [a], R. Sot [b], V. Pierron-Bohnes [c]

[a] Interdisciplinary Centre for Materials Modelling, M. Smoluchowski Institute of Physics, Jagellonian University, Reymonta 4, 30-059 Krakow, Poland
[b] Interdisciplinary Centre for Mathematical and Computational Modelling, University of Warsaw, Pawinskiego 5a, 02-106 Warsaw, Poland
[c] Institut de Physique et Chimie des Matériaux de Strasbourg, 23 rue du Loess, BP43 67034 Strasbourg, France

ARTICLE INFO

Article history:
Received 27 October 2009
Received in revised form
26 May 2010
Accepted 11 August 2010
Available online 16 September 2010

Keywords:
D. Defects
E. Simulations, Monte Carlo
E. Simulations, atomistic
E. Defects: theory
A. Nickel aluminides, based on NiAl

ABSTRACT

Lattice-gas decomposition model for equilibrium vacancy concentration in B2-ordered triple defect A–B binary intermetallic systems previously formulated and solved within the Bragg–Williams approximation was now simulated by means of Semi-Grand Canonical Monte Carlo (SGCMC) technique. Simulations of a ternary Ising lattice gas A–B–V with pair-interaction energies promoting the generation of A-antisites and A-vacancies revealed a miscibility gap and a coexistence of vacancy-poor and vacancy-rich phases within a wide range of temperature. The B2-ordered vacancy-poor phases were identified with intermetallic compounds containing equilibrium number of vacancies, which, at sufficiently low temperature, resulted proportional to the number of antisite defects. The latter effect additionally accompanied by the presence of constitutional vacancies in B-rich systems was interpreted as a signature of triple defect formation. The reliability of the model was checked by its implementation with Ni–Al EAM potential and by comparing the calculated vacancy concentrations in NiAl with the available experimental data. The modelled temperature dependence of the equilibrium vacancy concentration and configuration in triple defect B2-ordering binary intermetallics will be applied in Kinetic Monte Carlo (KMC) simulations of "order–order" kinetics in these systems.

1. Introduction

The presented study is a continuation of the previous one [1] reporting on the modelling of point defect thermodynamics in B2-ordered AB intermetalics. The works particularly address NiAl, a compound of interest as a basis of promising construction materials, which is a typical B2-ordering triple defect system showing outstandingly high vacancy concentration [2]. Surprisingly, the vacancy-mediated "order–order" kinetics is in this system much slower than e.g. in Ni_3Al containing by 7 orders of magnitude less vacancies [3]. The preliminary idea for explaining the effect pointed at the fact that antisite defects in NiAl are predominantly generated as triple defects, which means that: (i) Ni-antisite and Ni-vacancy formation energies are markedly lower than the corresponding formation energies for Al-antisites and Al vacancies, (ii) vacancy and antisite concentrations are correlated: two Ni-vacancies statistically associated with one Ni-antisite, (iii) vacancies reside preferentially on Ni-sublattice; their intersublattice jumps being energetically costly. Consequently, numerous vacancies generated in a triple defect B2 system are much less efficient as disordering agents than few vacancies in a non-triple defect system, also in $L1_2$-ordering Ni_3Al.

With reference to our previous papers (see e.g. Ref. [4]) it is intended to model the process by means of KMC simulations. In view, however, of high vacancy concentration correlated with the degree of long-range order (antisite concentration), standard simulations performed with a fixed number of vacancies are no longer justified and the implementation of complete vacancy thermodynamics – i.e. temperature dependence of vacancy concentration, is definitely required. The elaboration and solution of a related model constitutes the first stage of the project.

Similarly as in the previous paper [1] vacancy thermodynamics is considered within a model originally proposed by Schapink [5]. In this approach a lattice gas composed of atoms and vacancies and isostructural with the considered system decomposes into vacancy-rich and vacancy-poor phases, the latter one being identified with the system in question containing equilibrium number (concentration) of vacancies.

* Corresponding author.
E-mail address: biborski@wp.pl (A. Biborski).

0966-9795/$ – see front matter © 2010 Elsevier Ltd. All rights reserved.
doi:10.1016/j.intermet.2010.08.007

The previous study [1], where the model was solved within the Bragg–Williams (B–W) approximation, addressed specifically B2 A–B binary systems with energetically induced preference for A-antisite and A-vacancy formation. A wide space of atom–atom and atom–vacancy pair interactions was scanned and a range of interactions was found, for which antisite and vacancy concentrations C_{ant} and C_V were proportional:

$$\frac{C_{ant}(T)}{C_V(T)} = \frac{1}{2} \tag{1}$$

within finite intervals of temperature T.

The above effect was recognised as a signature for triple defect formation. It is interesting that the proportionality (1) was observed for appropriate pair-interaction energies in stoichiometric AB systems, as well as in non-stoichiometric, both A-rich and B-rich ones. In the case of the B-rich systems constitutional vacancies remained at $T \to 0$ K and at $T > 0$ K the proportionality (1) held only for thermally activated defects. In parallel with the manifestation of triple defect formation (Eq. (1)), the model yielded temperature dependencies $C_V^{(A)}(T)$ and $C_V^{(B)}(T)$ of A- and B-vacancy concentrations – the most interesting from the point of view of the general project. All the results followed directly from the B–W solution of the thermodynamic model without any a priori assumptions of e.g. the absence of B-vacancies, often made in literature.

Despite the promising results, implementation of the elaborated B–W vacancy thermodynamics in the KMC simulations for ordering kinetics (yielding in principle an exact solution of the pair-interaction Ising-type model) would undoubtedly violate the consistency of the whole research.

The present paper presents the solution of the "lattice-gas" model of vacancy thermodynamics in B2 triple defect binaries by means of Semi-Grand Canonical Monte Carlo (SGCMC) simulations. As shown in the following, the solution qualitatively reproduced the main B–W results and yielded discretised $C_V(T)$ dependence – directly applicable in the future KMC simulations. The preliminary results of the SGCMC simulations have recently been presented on the MRS Fall Meeting 2008 [6].

2. SGCMC simulations of ternary A–B–V B2-ordering lattice gas

2.1. Principles

The methodology followed standard Monte Carlo techniques steming from the idea of Binder et al. [7] and developed by many authors for the sake of phase diagram determination (see e.g. [8–13]). The procedure consists of the search for a set $\{\mu_i\}$ of chemical potentials of the system components corresponding to more than one composition of an open system. To the authors' knowledge, such a method has up to now never been used in the field of vacancy thermodynamics. The previous Monte Carlo-based approaches to the problem (see e.g. papers of Lim et al. [14,15]) were conceptually different.

In the present study the Semi-Grand Canonical Ensemble of the A–B–V B2-ordering lattice gases was considered – i.e. variation of the gas composition was constrained by a fixed total number $\overline{N}$ of the particles (i.e. lattice sites). In view of the fixed volume following from the rigid-lattice approach the equilibrium composition and configuration of the gas is thus determined at temperature T and the chemical potentials $\{\mu_i\}$ $(i = A,B,V)$ of the component species by a minimum of the Grand Potential functional Ω:

$$\Omega(T, \{\mu_i\}, \{\overline{\rho}\}, \{\overline{N}_i\}) = F(T, \{\overline{\rho}\}, \{\overline{N}_i\}) - \sum_i \mu_i \overline{N}_i \tag{2}$$

where F, $\{\overline{\rho}\}$ and $\overline{N}_i$ denote the free energy, set of variables – e.g. cluster variables parameterizing the chemical configuration and the number of i-type particles, respectively.

It obviously holds: $\sum_i \overline{N}_i = \overline{N}$.

Because of fixed $\overline{N}$ it is convenient to handle functions and parameters calculated per one particle:

$$\frac{\Omega}{\overline{N}} = \omega(T, \{\mu_i\}, \{\overline{\rho}\}, \{\overline{C}_i\}) = f(T, \{\overline{\rho}\}, \{\overline{C}_i\}) - \sum_i \mu_i \overline{C}_i \tag{3}$$

where $\overline{C}_i$ denotes the concentration of i-species in the lattice gas.

The equilibrium state of the lattice gas corresponding to the minimum of ω is produced by Semi-Grand Canonical Monte Carlo (SGCMC) simulations run for particular T and $\{\mu_i\}$ by means of the following algorithm [8]:

- Random choice of a single lattice site (the site is occupied by a species "p" (A-atom, B-atom or vacancy V),
- Random choice of a species type "q",
- Replacement of the species "p" by the species "q" with Metropolis probability:

$$\Pi_{p\to q} = \min\left\{1, \exp\left[-\frac{\Delta E_{p\to q} - (\mu_q - \mu_p)}{k_B T}\right]\right\} \tag{4}$$

where $\Delta E_{p\to q}$ denotes the change of the system configurational energy due to the $p \to q$ replacement. It is evaluated within a particular model of the system implemented with the simulations and depends on the current composition and configuration of the gas.

As follows from Eq. (4) (which is a consequence of fixed $\overline{N}$), the problem is effectively parameterised by differences of chemical potentials. In the following considerations two independent parameters are used:

$$\Delta\mu_{AV} = \mu_A - \mu_V \tag{5}$$

$$\Delta\mu_{BV} = \mu_B - \mu_V$$

A series of SGCMC runs carried out in the way that the $(\Delta\mu_{AV}, \Delta\mu_{BV})$ plane is scanned for fixed T results in equilibrium $\{\overline{C}_{i,T}(\Delta\mu_{AV}, \Delta\mu_{BV})\}$ and $\{\overline{\rho}_T(\Delta\mu_{AV}, \Delta\mu_{BV})\}$ isotherms.

Possible decomposition of the lattice gas into vacancy-poor and vacancy-rich phase within a miscibility gap is equivalent to a discontinuous phase transition generated at temperature T by the

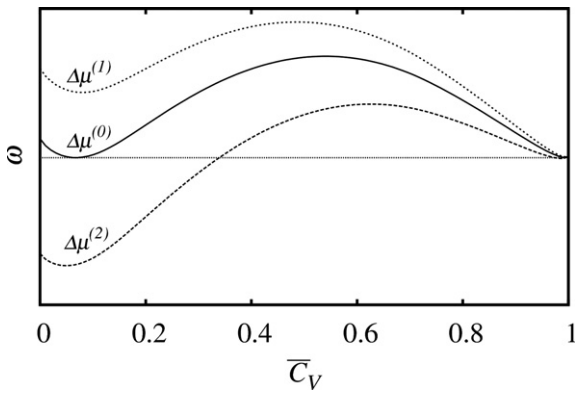

Fig. 1. $\overline{C}_A = \overline{C}_B$ sections of the concentration dependence of the B–W A–B–V lattice gas ω functional at $T/T_C = 0.53$ (where T_C is order–disorder temperature – see also Section 4.1.1). The curves were calculated for three values of $\Delta\mu = \mu_V - (\mu_A + \mu_B)/2$. The discontinuous phase transition occurs at $\Delta\mu = \Delta\mu^{(0)}$.

field of $\Delta\mu_{AV}$ and $\Delta\mu_{BV}$ and occurring between configurations determined by distinct minima of ω. At the transition point ($\Delta\mu_{AV}^{(0)}$, $\Delta\mu_{BV}^{(0)}$) determining the relative chemical potentials in the co-existing phases, the minima become equal (Eq. (3), Fig. 1).

According to the Gibbs phase rule, at each temperature the transition points related to *two-phase* equilibria form a line on the ($\Delta\mu_{AV}$, $\Delta\mu_{BV}$) surface. Possible three- or more phase equilibria (never detected within the present study) would, of course, be represented at particular temperatures by single points on the ($\Delta\mu_{AV}$, $\Delta\mu_{BV}$) surface.

The above discontinuous phase transitions show up as characteristic "facets" on the respective $\{\overline{C}_{i,T}(\Delta\mu_{AV}, \Delta\mu_{BV})\}$ and $\{\overline{\rho}_T(\Delta\mu_{AV}, \Delta\mu_{BV})\}$ isotherms. In fact, however, the occurrence of metastable configurations results in a hysteresis of facet positions and accurate determination of the ($\Delta\mu_{AV}^{(0)}$, $\Delta\mu_{BV}^{(0)}$) points requires specific techniques described in subsequent sections.

In view of the particular interest of the present study, analysed are mainly $\overline{C}_{V,T}(\Delta\mu_{AV}, \Delta\mu_{BV})$ isotherms as shown in Fig. 2.

The lower one of the two $\overline{C}_{V,T}(\Delta\mu_{AV}^{(0)}, \Delta\mu_{BV}^{(0)})$ solutions is identified with the equilibrium vacancy concentration $C_V(T)$ in an A–B crystal with C_A/C_B ratio determined by the point ($\Delta\mu_{AV}^{(0)}$, $\Delta\mu_{BV}^{(0)}$).

2.2. Details of the simulation technique

The lattice gas was simulated by generating a B2 supercell (Fig. 3) with periodic boundary conditions.

The supercell was built of $15 \times 15 \times 15$ bcc unit cells (i.e. with 6750 lattice sites), whose A- and B-sublattice sites (Fig. 3) were filled with A-atoms, B-atoms and vacancies.

The study was pursued by repeating the following sequence of steps at a series of temperatures (Fig. 4):

- Determination of temperature T,
- Preliminary localisation of the $\overline{C}_{V,T}(\Delta\mu_{AV}, \Delta\mu_{BV})$ facet by scanning a mesh of the entire ($\Delta\mu_{AV}$, $\Delta\mu_{BV}$) surface; each simulation starting from the perfect B2 configuration of the supercell with $\overline{C}_A = \overline{C}_B = 1/2; \overline{C}_V = 0$
- Determination of $S_{\Delta\mu}^{(\delta)}$ lines on the ($\Delta\mu_{AV}$, $\Delta\mu_{BV}$) surface corresponding to fixed selected equilibrium ratios $\delta = \overline{C}_B/(\overline{C}_A + \overline{C}_B)$ (Fig. 4a);
- Accurate analysis of the facet by pursuing chains of "step-by-step" SGCMC simulations (see e.g. [10]) along particular $S_{\Delta\mu}^{(\delta)}$ lines crossing the $\overline{C}_{V,T}(\Delta\mu_{AV}, \Delta\mu_{BV})$ facet (point A in Fig. 4): each simulation starting from a configuration produced by the preceding one. The facets were crossed in both directions, which resulted in hysteresis mentioned in Section 2 (Fig. 4b).

The resulting system configuration was analysed by monitoring MC time dependence of the values of $\overline{N}_A, \overline{N}_B, \overline{N}_V$ and of the LRO and SRO parameters defined as:

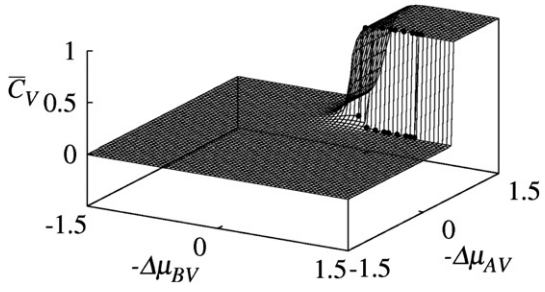

Fig. 2. Typical $\overline{C}_{V,T}(\Delta\mu_{AV}, \Delta\mu_{BV})$ isotherm with a facet showing the discontinuous phase transition.

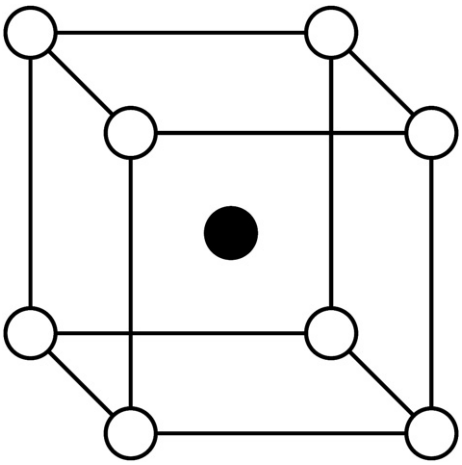

Fig. 3. Scheme of B2 superstructure: ● A-sublattice, ○ B-sublattice.

$$\overline{\eta}_A = \frac{\frac{\overline{N}_A^{(A)}}{\frac{1}{2}\overline{N}} - \overline{C}_A}{\frac{\overline{N}_A}{\frac{1}{2}\overline{N}} - \overline{C}_A} = \frac{2\overline{N}_A^{(A)} - \overline{N}_A}{\overline{N}_A} \tag{6}$$

$$\overline{\eta}_V = \frac{\frac{\overline{N}_V^{(A)}}{\frac{1}{2}\overline{N}} - \overline{C}_V}{\frac{\overline{N}_V}{\frac{1}{2}\overline{N}} - \overline{C}_V} = \frac{2\overline{N}_V^{(A)} - \overline{N}_V}{\overline{N}_V} \tag{7}$$

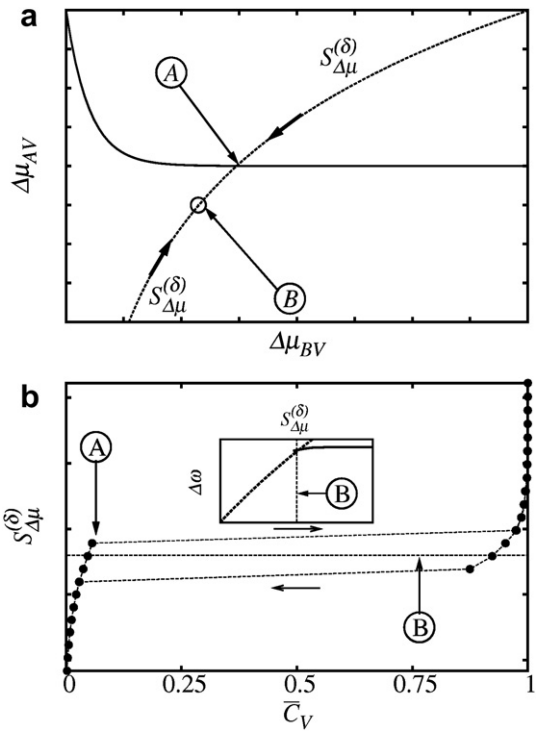

Fig. 4. Scheme of the method for the evaluation of vacancy concentration: (a) Solid line represents the trace of $\overline{C}_{V,T}(\Delta\mu_{AV}, \Delta\mu_{BV})$ facet, which is crossed at the point A by $S_{\Delta\mu}^{(\delta)}$ path. Point B ($\Delta\mu_{AV}^{(0)}, \Delta\mu_{BV}^{(0)}$) is determined by means of thermodynamic integration of the Grand Potential ω along $S_{\Delta\mu}^{(\delta)}$; (b) $S_{\Delta\mu}^{(\delta)}(\overline{C}_V)$ hysteresis. The inset shows a typical result of the thermodynamic integration.

$$\overline{\eta}_{\mathrm{B}} = \frac{\frac{\overline{N}_{\mathrm{B}}^{(\mathrm{B})}}{\frac{1}{2}\overline{N}} - \overline{C}_{\mathrm{B}}}{\frac{\overline{N}_{\mathrm{B}}}{\frac{1}{2}\overline{N}} - \overline{C}_{\mathrm{B}}} = \frac{2\overline{N}_{\mathrm{B}}^{(\mathrm{B})} - \overline{N}_{\mathrm{B}}}{\overline{N}_{\mathrm{B}}} = \frac{\overline{N}_{\mathrm{A}}}{\overline{N}_{\mathrm{B}}} \times \overline{\eta}_{\mathrm{A}} + \frac{\overline{C}_{\mathrm{V}}\left(1 + \frac{\overline{N}_{\mathrm{A}}}{\overline{N}_{\mathrm{B}}}\right)}{1 - \overline{C}_{\mathrm{V}}} \times \overline{\eta}_{\mathrm{V}} \qquad (8)$$

$$\overline{\alpha}_{\mathrm{A}} = \frac{\sum_{i=1}^{\overline{N}_{\mathrm{A}}^{(\mathrm{B})}} n_{v,i}}{\overline{N}_{\mathrm{A}}^{(\mathrm{B})}} \qquad (9)$$

where $\overline{N}_i^{(\sigma)}$ denotes the number of i-type atoms occupying σ-sublattice sites and $n_{v,I}$ denotes the number of vacancies being nearest neighbours of an i-th A-antisite.

Each simulation run was continued until a saturation of the monitored parameters was observed for 60% of the total number of SGCMC steps and the equilibrium values of the parameters were evaluated by taking arithmetic means from sets of randomly probed values appearing after the saturation of the corresponding simulated MC time dependence (the averaging was done with a special care so that possible correlations between the values are eliminated).

The range of T was limited at the bottom by the low rate of the SGCMC curve saturation and at the top by the critical temperature of the miscibility gap of the A–B–V lattice gas.

Two procedures were applied to determine accurate values of $(\Delta\mu_{\mathrm{AV}}^{(0)}, \Delta\mu_{\mathrm{BV}}^{(0)})$ (point B in Fig. 4) corresponding to the discontinuous phase transformation of the system and to the equilibrium coexistence of the vacancy-poor and vacancy-rich phases of the lattice gas: At low T, where the minima of $\omega(\overline{C}_{\mathrm{V}})$ were localised at $\overline{C}_{\mathrm{V}} \ll 1$ and $\overline{C}_{\mathrm{V}} \approx 1$ the thermodynamic integration method proposed by Dünweg et al. [9] was performed along the $S_{\Delta\mu}^{(\delta)}$ curves (see the inset in Fig. 4b). Its reliability followed from the reference states (from which the integration starts) to be safely chosen as an A–B binary with no thermal vacancies and a purely vacant bcc lattice gas. The results showed, however, that with increasing T the hysteresis continuously shrunk and the values of $\Delta\mu_{\mathrm{AV}}^{(0)}$ and $\Delta\mu_{\mathrm{BV}}^{(0)}$ resulted close to the arithmetic means of its limits. Simultaneously, the accuracy of the thermodynamic integration method deteriorated (see Section 4.1.1) and, therefore, the values of $\Delta\mu_{\mathrm{AV}}^{(0)}$ and $\Delta\mu_{\mathrm{BV}}^{(0)}$ corresponding to $T/T_{\mathrm{C}} > 0.47$ were estimated as arithmetic means of the hysteresis limits.

Finally, the equilibrium vacancy concentration C_{V}, as well as the equilibrium values of the LRO and SRO parameters η_{A}, η_{B}, η_{V} and α_{A} in the $A_{1-\delta}B_{\delta}$ system at temperature T were identified with those associated with the phase showing the lower value of $\overline{C}_{\mathrm{V}}$ corresponding to $(\Delta\mu_{\mathrm{AV}}^{(0)}, \Delta\mu_{\mathrm{BV}}^{(0)})$.

3. Lattice gas Hamiltonian

Two particular models of the lattice gas were implemented:

- The Ising-type model with nearest neighbour (nn) pair interactions applied in the previous paper [1] to B2 triple defect A–B systems.
- The embedded-atom (EAM) model elaborated by Mishin et al. [16] for Ni–Al systems.

3.1. Ising-type model

The energy change $\Delta E_{p\to q}$ (Eq. (4)) was given by

$$\Delta E_{p\to q} = \sum_{i\geq j} \Delta N_{ij}^{(p\to q)} \times V_{ij} \qquad (10)$$

where $i,j = \mathrm{A,B,V}$; V_{ij} denotes nn i/j pair-interaction energy and $\Delta N_{ij}^{(p\to q)}$ denotes the change of the number of nn i–j pairs in the system caused by the $p \to q$ exchange.

As briefly mentioned in Section 1, when solving the model within the B–W approximation [1] the adequacy of nn pair potentials V_{ij} in promoting triple defect formation was reflected by a resulting proportionality between antisite and vacancy concentrations in a possibly wide temperature range. It was found that the appropriate parameters controlling the effect were:

$$\frac{V_{\mathrm{asym}}}{W} = \frac{V_{\mathrm{AA}} - V_{\mathrm{BB}}}{2V_{\mathrm{AB}} - V_{\mathrm{AA}} - V_{\mathrm{BB}}} \qquad (11a)$$

and

$$\frac{V_{\mathrm{AV}}}{W} = \frac{V_{\mathrm{AV}}}{2V_{\mathrm{AB}} - V_{\mathrm{AA}} - V_{\mathrm{BB}}} = \frac{-V_{\mathrm{BV}}}{W} \qquad (11b)$$

The triple defect formation was found for $V_{\mathrm{asym}}/W > 0.4$ and $V_{\mathrm{AV}}/W > -0.3$ (see Fig. 9 in Ref. [1]). Particular values of the parameters (necessary for effective calculations) were chosen rather arbitrarily by putting: $W = -0.08$ eV (the value yielding "order–disorder" temperature $T_{\mathrm{C}} \approx 1850$K in the AB system without vacancies), $V_{\mathrm{BB}} = -0.05$ eV and $V_{\mathrm{VV}} = 0$. For the sake of the present study, V_{ij} parameters were evaluated with reference to the B–W results: $V_{\mathrm{asym}}/W = 0.875$, $V_{\mathrm{AV}}/W = -V_{\mathrm{BV}}/W = -0.5$. Correspondingly, the following values of the nn pair-interaction parameters were applied:

$$V_{\mathrm{AA}} = -0.12\ \mathrm{eV} \quad V_{\mathrm{BB}} = -0.05\ \mathrm{eV} \quad V_{\mathrm{VV}} = 0.0\ \mathrm{eV} \qquad (12)$$

$$V_{\mathrm{AB}} = -0.125\ \mathrm{eV} \quad V_{\mathrm{AV}} = +0.04\ \mathrm{eV} \quad V_{\mathrm{BV}} = -0.04\ \mathrm{eV}$$

3.2. EAM model

The EAM potential derived for Ni–Al [16] was implemented with SGCMC simulations of NiAl. The potential was first tested for the reproducibility of the fundamental parameters of NiAl and then the simulations were run with the energy difference $\Delta E_{p\to q}$ (Eq. (4)) calculated within a sphere covering 6 co-ordination zones of the probed site.

4. Results

4.1. Ising A–B–V lattice gas model

4.1.1. General results

In qualitative consistency with the previous paper [1] detailed analysis was done for three systems: $A_{0.52}B_{0.48}$-V ($\delta = 0.48$), $A_{0.5}B_{0.5}$-V ($\delta = 0.5$) and $A_{0.48}B_{0.52}$-V ($\delta = 0.52$). The greater departures from stoichiometry (with respect to those applied in Ref. [1]) were required because of the resolution $\Delta\delta \geq 0.1$ of the determination of $S_{\Delta\mu}^{(\delta)}$ lines (see Section 2.2). It was found out that while at low temperatures the co-existing vacancy-poor and vacancy-rich phases showed equal values of δ (i.e. the gas decomposed along tie lines oriented towards the V corner of the Gibbs triangle), this was not exactly the case at temperatures close to the critical (consolute) point. Although the tilt of the tie-line orientation was quite slight, it was no longer strictly possible to identify particular $A_{1-\delta}B_{\delta}$ systems with vacancies as resulting from the decomposition of the same lattice gas in the whole temperature range. Fig. 5 shows three sections of the miscibility gap of the A–B–V lattice gas as revealed by the SGCMC simulations. Only the vacancy-poor borders of the sections correspond, however, in each case to strictly constant δ. The diagrams are scaled in a reduced-temperature T/T_{C}, where $T_{\mathrm{C}}(\delta)$ denotes "order–disorder" transition points determined for particular $A_{1-\delta}B_{\delta}$ systems (see Section 4.1.2).

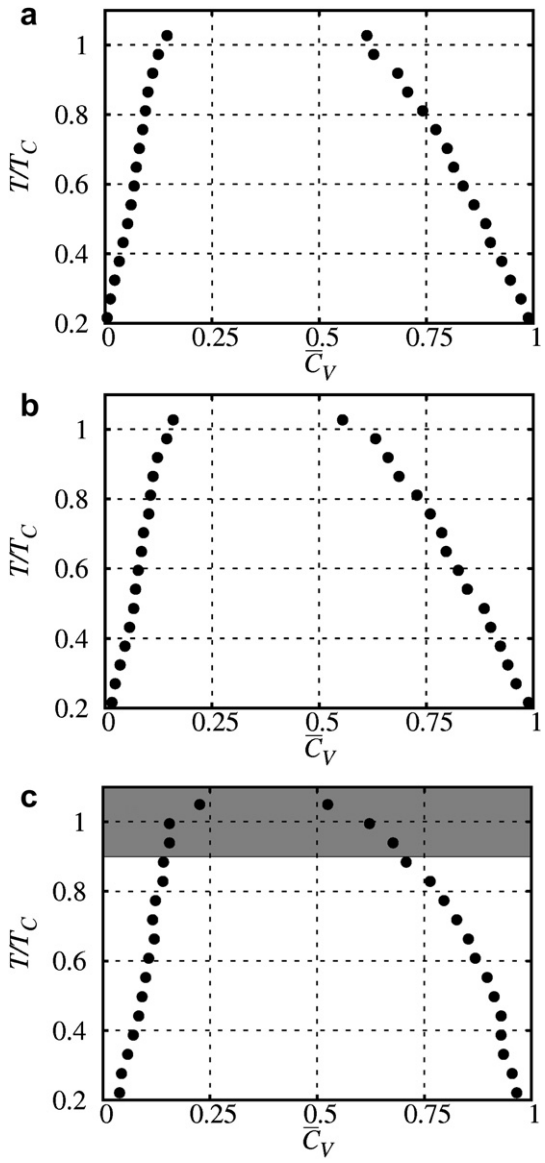

Fig. 5. Sections of the miscibility gap of the A–B–V lattice gas. Vacancy-poor borders of the sections correspond to: (a) $A_{0.52}B_{0.48}$–V ($\delta = 0.48$); (b) $A_{0.5}B_{0.5}$–V ($\delta = 0.5$); (c) $A_{0.48}B_{0.52}$–V ($\delta = 0.52$).

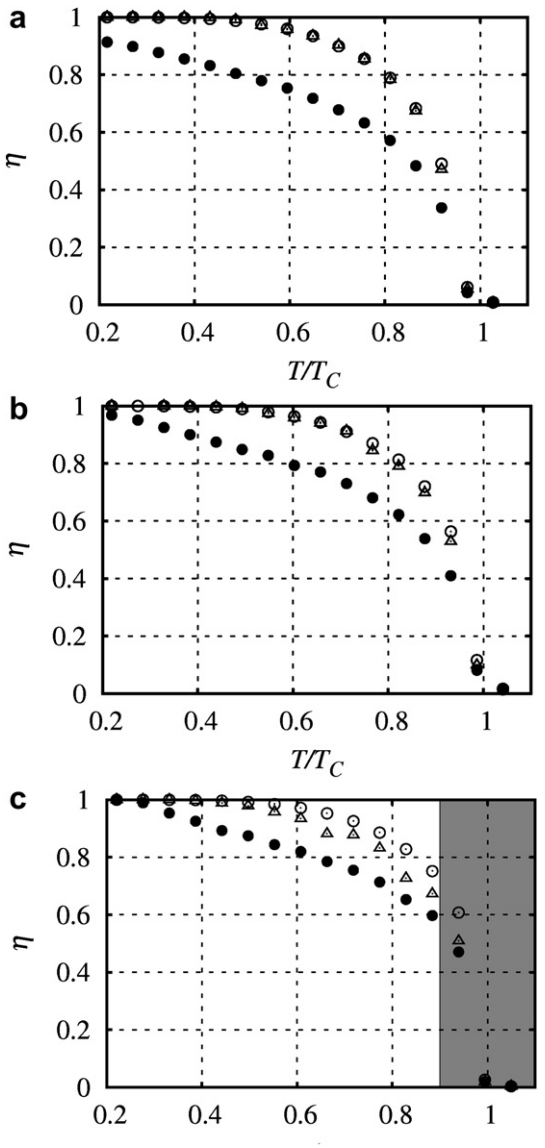

Fig. 6. Reduced-temperature dependences of LRO parameters in (a) $A_{0.52}B_{0.48}$; (b) $A_{0.5}B_{0.5}$; (c) $A_{0.48}B_{0.52}$. ● η_A, ○ η_B, Δ η_V.

As follows in addition from Fig. 5c, the critical point of the $A_{0.48}B_{0.52}$-V section of the miscibility gap appeared close to T_C, which generated especially high uncertainty of the related SGCMC results (grey area in Figs.5c, 6c, 7c, 8c, 9e and f).

4.1.2. Long-range order

Continuous B2 ↔ A2 "order–disorder" transition was observed in all the three $A_{1-\delta}B_\delta$ binary systems examined. While all the η_A, η_B and η_V LRO parameters reached zero value at the same temperature T_C ($T_C = -1.72 \times W/k_B$ for $\delta = 0{,}5$), their temperature dependences differed one from another showing the definite preference for A-antisite formation at $T < T_C$ (Fig. 6).

4.1.3. Correlated vacancy and antisite concentration and configuration

As follows from the phase diagrams (Fig. 5) the total vacancy concentration C_V increased with temperature showing the highest value in $A_{0.48}B_{0.52}$.

Vacancies were generated predominantly on the A-sublattice (almost only A-vacancies formed at lower temperatures). The coincidence of the $C_V^{(A)}(T/T_C)$ and $C_V^{(B)}(T/T_C)$ curves at $T/T_C = 1$ was due to a decrease of $C_V^{(A)}$ close to T_C (Fig. 7). The concentration $C_V^{(A)}$ of A-vacancies remaining in $A_{0.48}B_{0.52}$ down to the lowest temperatures (Fig. 7c) was definitely higher than in the case of $\delta = 0.48$ and $\delta = 0.5$ (Fig. 7a and b).

The asymmetric increase of $C_V^{(A)}$ and $C_V^{(B)}$ with increasing temperature was accompanied by a similar behaviour of antisite concentrations $C_A^{(B)}$ and $C_B^{(A)}$ (Fig. 8) showing a markedly preferential formation of A-antisites. In the case of the system $A_{0.52}B_{0.48}$ the concentration $C_A^{(B)}$ of A-antisites remaining down to the lowest temperature was definitely the highest (Fig. 8a).

4.1.4. Triple defect formation

Following the idea of our previous paper [1], the simulation results were inspected for triple defect formation by analysing temperature dependencies of the ratio of antisite and vacancy concentrations. The results are shown in Fig. 9, where three variants of the "triple defect indicator" *TDI* were defined as follows:

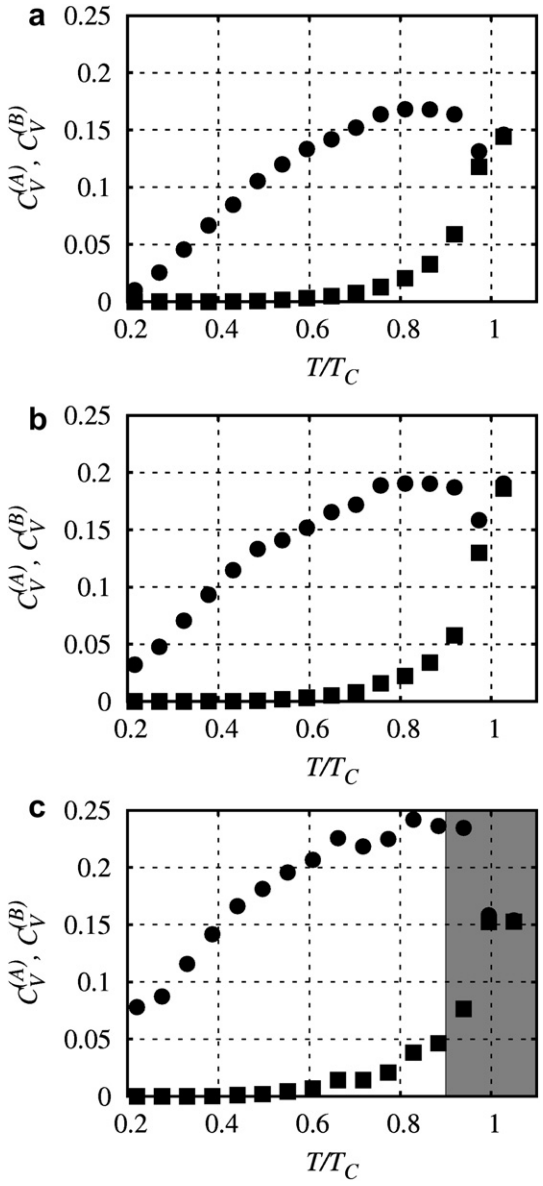

Fig. 7. Reduced-temperature dependences of vacancy concentrations on sublattices in: (a) $A_{0.52}B_{0.48}$; (b) $A_{0.5}B_{0.5}$; (c) $A_{0.48}B_{0.52}$, ● $C_V^{(A)}$, ■ $C_V^{(B)}$.

$$TDI = \frac{C_A^{(B)} + C_B^{(A)}}{C_V} \tag{13}$$

$$TDI_{ACT} = \frac{\left(C_A^{(B)} - C_A^{(B)}(T\to 0)\right) + \left(C_B^{(A)} - C_B^{(A)}(T\to 0)\right)}{C_V - C_V(T\to 0)} \tag{14}$$

$$TDI_{ACT}^{(A)} = \frac{\left(C_A^{(B)} - C_A^{(B)}(T\to 0)\right)}{C_V^{(A)} - C_V^{(A)}(T\to 0)} \tag{15}$$

Formulae (14) and (15) define *TDI* parameters accounting exclusively for thermally activated vacancies and antisites – i.e. with subtracted concentrations of constitutional defects.

Well-marked plateaux of $TDI_{ACT} = 1/2$ and $TDI_{ACT}^{(A)} = 1/2$ were observed for finite temperature ranges for all the three examined systems (in the case of $\delta = 0.5$ $TDI = TDI_{ACT}$). In contrary, no plateaux were shown by the TDI curves in the case of $A_{0.52}B_{0.48}$ and $A_{0.48}B_{0.52}$.

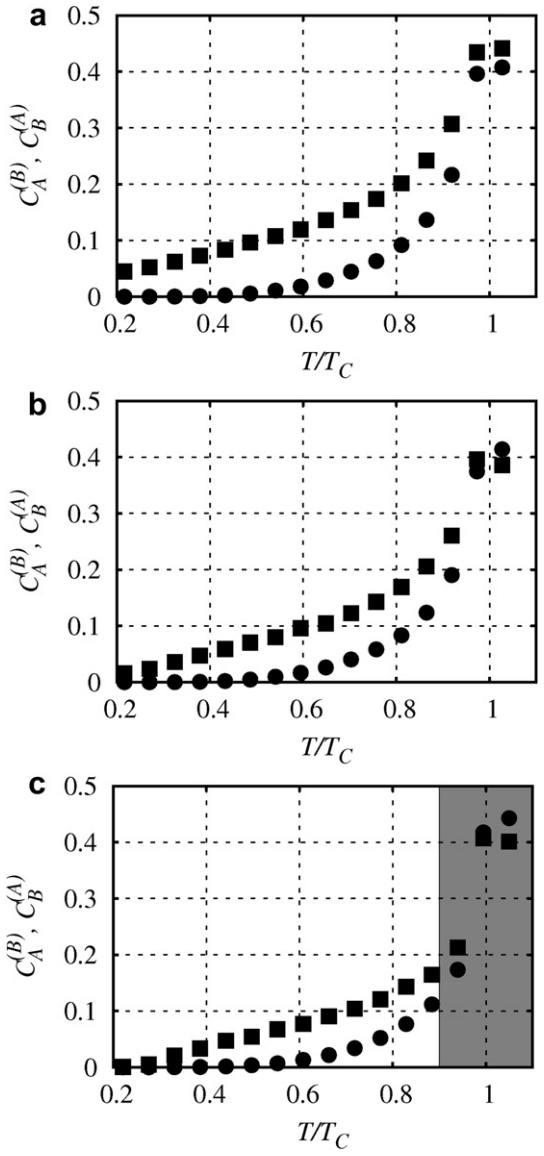

Fig. 8. Reduced-temperature dependences of antisite concentrations in: (a) $A_{0.52}B_{0.48}$; (b) $A_{0.5}B_{0.5}$; (c) $A_{0.48}B_{0.52}$: ■ $C_A^{(B)}$, ● $C_B^{(A)}$.

The result is in agreement with the previous one obtained within the B–W approximation [1] and indicates that the correlated triple defect-like *thermal* generation of vacancies and antisite defects in the system takes place on both sides of the stoichiometric composition $A_{0.5}B_{0.5}$. An increasing temperature disturbs the correlation in the way that antisite generation becomes predominating. Comparison of the TDI_{ACT} and $TDI_{ACT}^{(A)}$ curves (wider temperature range for $TDI_{ACT}^{(A)}$ plateau) shows in addition that the plateau disturbance is triggered by the activation of the energetically costly B-vacancy and B-antisite formation.

The character of the triple defects generated in the $A_{0.5}B_{0.5}$ system was examined by analysing the temperature dependence of the SRO parameter α_A (Eq. (13), Fig. 10).

Despite an increase with increasing temperature α_A resulted always definitely lower than 1 – in particular, in the temperature range of the *TDI* plateau (Fig. 9c, d). This means that the triple defects were of purely statistical character – i.e. no nn complexes of two A-vacancies and one A-antisite were generated. This result, though being a natural consequence of $V_{AV} > 0$ (Eq. (12)), is not trivial, which will be discussed in Section 5.

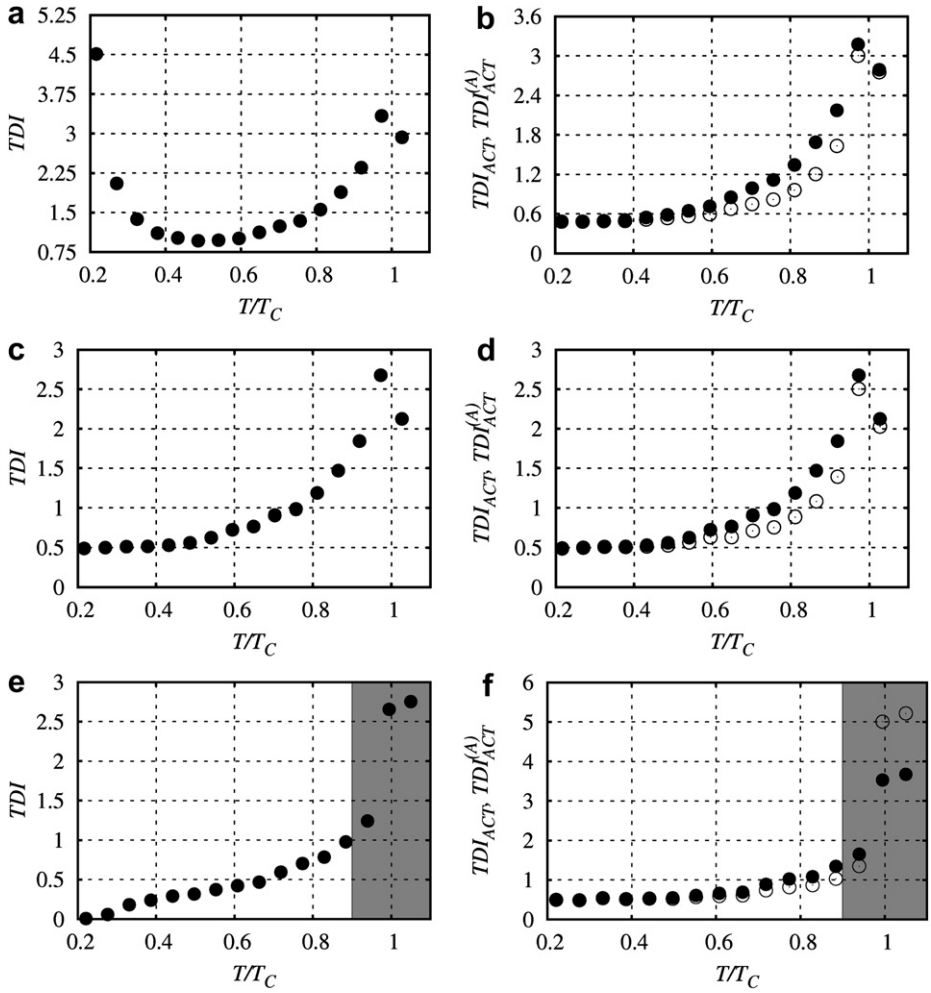

Fig. 9. Reduced-temperature dependence of Triple Defect Indicators *TDI*. $A_{0.52}B_{0.48}$: (a) *TDI*, (b) ● TDI_{ACT}, ○ $TDI^{(A)}_{ACT}$; $A_{0.5}B_{0.5}$: (c) $TDI = TDI_{ACT}$, (d) $TDI^{(A)}_{ACT}$; $A_{0.48}B_{0.52}$: (e) *TDI*, (f) ● TDI_{ACT}, ○ $TDI^{(A)}_{ACT}$.

4.2. Reliability: EAM Ni–Al–V lattice gas model – comparison of C_V with experimental results

As announced in Section 3.2 equilibrium vacancy concentration at 1500 K was determined for NiAl by implementing the SGCMC procedure with the most recent EAM potentials elaborated for Ni–Al [16]. Effective interatomic interactions up to the 6th coordination zone were taken into account and a supercell built of $10 \times 10 \times 10$ B2 unit cells with periodic boundary conditions allowed the computations to be performed within a reasonable CPU time.

Fig. 11a shows the observed hysteresis loop analogous to the one of Fig. 4b indicating efficiency of the method now implemented with the EAM formalism.

It was found out that the EAM Ni–Al–V lattice gas decomposed into almost pure vacancies and almost perfectly B2-ordered NiAl with very low vacancy concentration. The thermodynamic integration procedure leading to the determination of $(\Delta\mu^{(0)}_{NiV}, \Delta\mu^{(0)}_{AlV})$ was thus simplified by putting constant $\Delta\omega = 0$ for the vacancy-reach phase (Fig. 11b).

Because of very low number of the vacancies generated in the vacancy-poor phase at $(\Delta\mu^{(0)}_{NiV}, \Delta\mu^{(0)}_{AlV})$ and consequently high level of fluctuations only the order of magnitude $C^{(A)}_V \propto 10^{-3}, C^{(B)}_V \approx 0$ was determined. The result was, however, in surprisingly good agreement with the value of C_V resulting from the extrapolation of the experimental data reported by Schaeffer et al. [2] to $T = 1500$ KK and even in better agreement with those obtained by Zobel (see Ref. [18] and reference therein).

The reliability of the above result suffers, however, from the negligence of lattice relaxation: the EAM potential was implemented in rigid-lattice SGCMC simulations. Further extension of the procedure upon e.g. lattice and atomic positions relaxation routine (see e.g. [19,20]) would force additional reduction of the sample size making the calculations definitely useless. Possible effect of the lattice relaxation on the resulting vacancy concentration in NiAl may, however, be roughly assessed by considering the

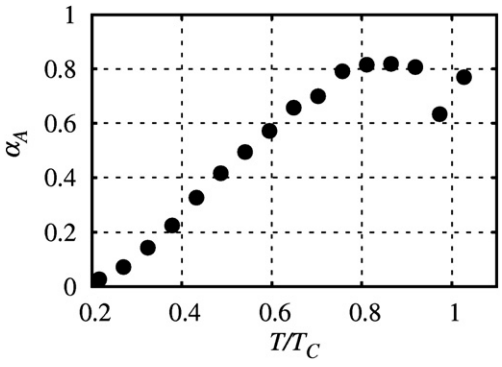

Fig. 10. Reduced-temperature dependence of the SRO parameter α_A in $A_{0.5}B_{0.5}$.

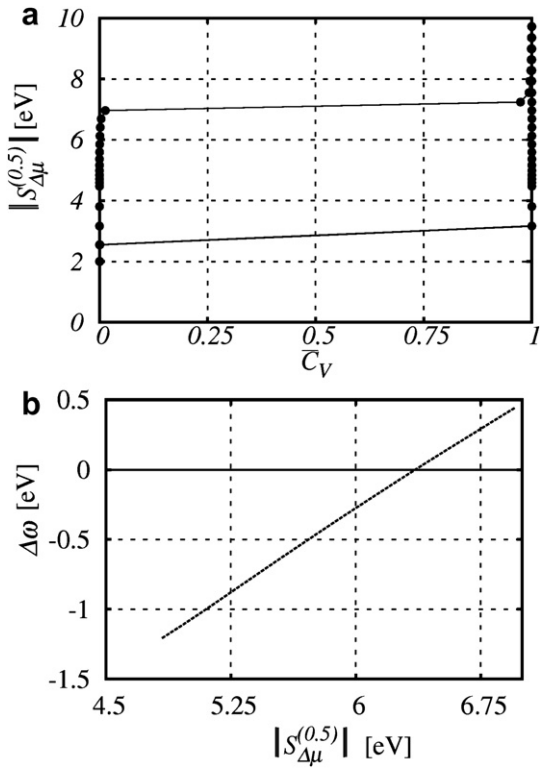

Fig. 11. SGCMC simulation of NiAl modelled with EAM energetics [16] at $T = 1500$ K: (a) $S_{\Delta\mu}^{(0.5)}(\overline{C}_V)$ hysteresis; (b) result of thermodynamic integration.

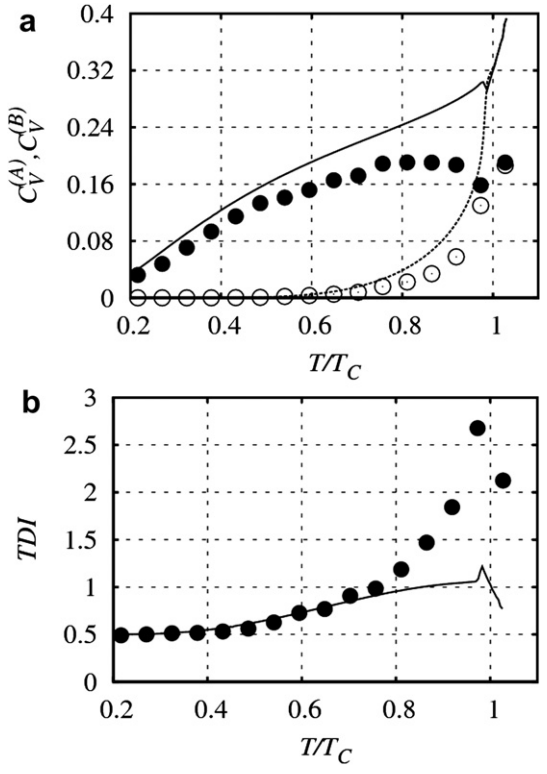

Fig. 12. Comparison of the SGCMC and B–W solution of the A–B–V Ising lattice gas model with nn pair-interaction parameters given by Eq. (15): (a) SGCMC $C_V^{(A)}$ ●; B–W $C_V^{(A)}$ solid line, SGCMC $C_V^{(B)}$ ○, B–W $C_V^{(B)}$ dashed line;(b) SGCMC *TDI* ●, B–W *TDI* solid line.

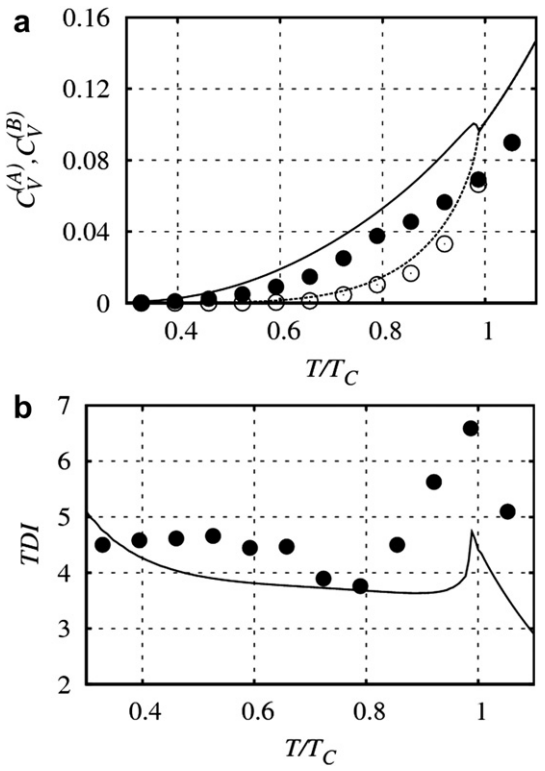

Fig. 13. Comparison of the SGCMC and B–W solution of the A–B–V Ising lattice gas model of Fig. 12 after putting $V_{AV} = V_{BV} = 0$: (a) SGCMC $C_V^{(A)}$ ●; B–W $C_V^{(A)}$ solid line, SGCMC $C_V^{(B)}$ ○, B–W $C_V^{(B)}$ dashed line; (b) SGCMC *TDI* ●, B–W *TDI* solid line.

values of triple defect formation energy calculated within the EAM formalism in relaxed and unrelaxed NiAl lattice:

$$E_{\mathrm{TD}}^{(\mathrm{relaxed})} = 2.28\ \mathrm{eV}\ [16];\ E_{\mathrm{TD}}^{(\mathrm{unrelaxed})} = 2.45\ \mathrm{eV}$$

Taking into account that both in Mishin et al. [16] and our calculations, NiAl shows pure triple defect behaviour – i.e. only Ni-vacancies are generated in correlation with Ni-antisites, standard exponential dependence of vacancy concentration C_V on C_{TD} may be reasonably assumed and:

$$\frac{C_{\mathrm{V}}^{(\mathrm{relaxed})}}{C_{\mathrm{V}}^{(\mathrm{unrelaxed})}}(T) \approx \exp\left[\frac{E_{\mathrm{TD}}^{(\mathrm{unrelaxed})} - E_{\mathrm{TD}}^{(\mathrm{relaxed})}}{k_{\mathrm{B}}T}\right] \tag{16}$$

At $T = 1500$ K the above ratio approximates 3.7, which means that lattice relaxation should not affect the order of magnitude of the estimated C_V.

It is remarkable that the fluctuating values of $C_V^{(A)}$ and $C_A^{(B)}$ yielded a stable level of $TDI_{ACT}^{(A)} = 1/2$, but the low value of $\alpha_A \propto 10^{-2}$ again indicated the statistical character of triple defects. The result is non-trivial because in contrary to the case of the Ising $A_{0.5}B_{0.5}$, the 0 K formation energy for nn triple defects was in the EAM NiAl by 4% *lower* than the formation energy for the statistical (separated) triple defects.

5. Discussion and conclusions

5.1. General remarks on the applied lattice-gas decomposition model

The lattice-gas decomposition model for equilibrium vacancy concentration in B2-ordering binary systems was solved by means of SGCMC simulations. The presented results correspond mainly to

the Ising gas with nn pair-interaction parameters used previously in the B–W approximation [1] and yielding the tendency for triple defect formation. The study should be regarded as modelling pure chemical ordering phenomena, which in a real system occur together with processes controlled by other degrees of freedom. In the case of the intermetallic compounds addressed by the study (first of all Ni–Al) the crystalline lattice appears less stable than the B2 superstructure and the system shows almost perfect LRO up to the melting point. Consequently, the scale of ordering phenomena observed in the real systems is very fine and their simulation modelling is impossible by means of samples with sizes allowing the results to be obtained within realistic CPU time. The concept of the modelling presented in the paper (aiming in the elucidation of the correlated generation of vacancies and antisite defects) was to look at the processes through a specific "magnifying glass", which consisted of the application of appropriately scaled system energetics. Realistic Ni–Al EAM potentials were applied only for the sake of a quantitative verification of the model. Because of the limited sample size, however, the number of the generated vacancies was so small that only the order of magnitude of their concentration was estimated – appearing in a good agreement with the experimental data.

In contrary to the preceding B–W approach [1] where particular quasi-binary (A–B)–V lattice gases with fixed δ were considered separately, the present SGCMC formalism was based on the analysis of the entire ternary A–B–V system. The approach lead to a more general interpretation of the lattice-gas decomposition model: A particular $A_{1-\delta}B_{\delta}$ crystal with equilibrium vacancy concentration should not be identified at each temperature with the vacancy-poor *product of the decomposition of a* $A_{1-\delta}B_{\delta}$–V *lattice gas*, but should rather be considered as a vacancy-poor $A_{1-\delta}B_{\delta}$–V *lattice gas phase being in equilibrium with a vacancy-rich* $A_{1-\delta 1}B_{\delta 1}$–V *one* with $\delta 1$ not necessarily equal to δ. Non-negligible tilt of the lattice-gas decomposition tie lines from the $\delta = \text{const}$ orientation was, however, observed only at temperatures close to T_C and thus, the previous procedure [1] may be regarded as an acceptable approximation.

5.2. Triple defect formation in B2-ordering A–B binary systems

The triple defect formation in $A_{1-\delta}B_{\delta}$ probed in the present paper by the 1/2 plateaux on the *TDI* (T/T_C), TDI_{ACT} (T/T_C) and $TDI_{ACT}^{(A)}$ (T/T_C) dependences was a consequence of the applied energetics (Ising and EAM) promoting the formation of A-atisites and A-vacancies. It is remarkable that in the case of the Ising energetics the *TDI* curves showed the 1/2 plateaux only after "reinforcing" the A-vacancy formation preference with repulsive A-atom-vacancy interaction.

An increase of temperature activated long-range disordering showing preferential generation of A-antisites (Figs. 6 and 8) accompanied by almost exclusive formation of A-vacancies (Fig. 7). Although the formation of B-antisites and B-vacancies was delayed in the temperature scale, the system disordered at a particular temperature T_C where all the LRO parameters (Eqs. (5–7)) reached simultaneously their zero values. The "order–disorder" transition exhibited a continuous character, which, due to the preferential generation of A-antisites and A-vacancies, induced the characteristic shape of the temperature dependencies $C_V^{(A)}(T/T_C)$ and $C_V^{(B)}(T/T_C)$of vacancy concentrations on A- and B-sublatticies (Fig. 7) – in particular, a decrease of $C_V^{(A)}$ in the vicinity of $T = T_C$ was observed. Lack of an experimental evidence of the effect follows from the fact that most of real triple defect systems show almost perfect LRO up to the melting point.

The vacancy concentration markedly depended on the system composition and gradually increased with increasing δ (Fig. 7). Remarkably, the antisite concentration manifested an inverted δ-dependence (Fig. 8). This result was directly related to the way the system compensated the departure from stoichiometric composition $\delta = 1/2$: while the deficit of A-atoms ($\delta > 1/2$) was predominantly compensated by A-vacancies, excess A-atoms ($\delta < 1/2$) predominantly occupied antisite positions on the B-sublattice. The effect has been well known as the formation of constitutional point defects (vacancies or antisites) whose concentration does not vanish at $T \to 0$ K. Such a behaviour may indeed be deduced from the graphs of Figs. 7c and 8a.

The analysis of TDI_{ACT} (T/T_C) curves (Fig. 9a–f) indicated that, similarly as in the B–W solution [1], the concentrations of *thermally activated* antisites and vacancies determined by SGCMC simulations remained in a constant proportion of 1/2 within finite low temperature intervals; the effect being observed both for $\delta < 1/2$ and $\delta > 1/2$. An increase of TDI_{ACT} at higher temperatures indicated that the equilibrium antisite concentration in the system was becoming higher than that resulting from triple defect formation and that "hybrid" defects (triple defects and single antisites) [17] were activated. The comparison of the TDI_{ACT} and $TDI_{ACT}^{(A)}$ curves (Fig. 9b,d,f) shows in addition that the hybridization of defects was mainly due to the activation of B-antisite and B-vacancy formation. The latter finding is of great importance for the planned KMC modelling of the "order–order" kinetics in the triple defect B2 A–B binaries as due the high energetic cost, the process of B-antisite and B-vacancy formation is supposed to be highly sluggish.

The final comment concerns the short-range antisite-vacancy correlations observed in the configurations generated in the samples by SGCMC simulations. As follows from the presented results, the statistical character of the created triple defects resulted not only from the simulations of an Ising system with nn pair-interaction energies naturally promoting the separation of A-antisites and A-vacancies, but also from the simulations of NiAl modelled with EAM energetics promoting nn triple defect complexes. The result apparently points at the importance of configurational entropy effects at non-zero temperatures. On the other hand, preliminary results of the "ab initio" analysis carried out in the ICM Centre, Warsaw University suggest that the separation of triple defects in NiAl leads rather to a *decrease* of the configurational energy [21]. Such a behaviour was also observed in the EAM-modelled FeAl [22].

5.3. SGCMC simulations and B–W approximaton

Results of studies of phase equilibria carried out within B–W approximation and by means of SGCMC simulations have been compared and discussed in diverse contexts (see e.g. Refs. [15,23]). The SGCMC results reported in the present paper appear in a full *qualitative* agreement with the B–W ones. Using an improved software enabling more accurate function minimization, the B–W $C_V^{(v)}(T/T_C)$ and *TDI* (T/T_C) curves have been re-calculated. Although the main conclusions reported in Ref. [1] remained definitely correct, the detailed shape of the new curves was modified. Fig. 12a,b shows the SGCMC and the new B–W $C_V^{(v)}(T/T_C)$ and *TDI* (T/T_C) curves obtained for the same Ising A–B–V lattice gas with nn pair-interaction parameters given by Eq. (12).

B–W calculations resulted in generally higher vacancy concentration and while the SGCMC $C_V^{(A)}$ curve decreased in the vicinity of the "order–disorder" transition point, the B–W one showed only an inflection. Both approaches yielded definite 1/2 plateau of *TDI* at $T/T_C < 0.5$ (Fig. 12b); the stronger increase of the SGCMC curve at higher temperatures followed again from the considerably lower SGCMC vacancy concentration close to $T = T_C$.

Quite similar qualitative agreement between the SGCMC and B–W results was achieved when removing atom-vacancy pair-interaction and putting $V_{AV} = V_{BV} = 0$ (Fig. 13).

The *TDI* curves in Fig. 13b illustrate in addition that neither SGCMC, nor B–W thermodynamics yielded definite triple defect-type chemical disordering in the Ising A–B–V lattice gas without non-zero nn atom-vacancy interactions.

Acknowledgment

The main author (A.B.) acknowledges financial support by the Polish Ministry of Science and Higher Education: Grant no. N N202 173635. The Ministry supported other authors (L.Z., R.K., R.S.) by Grant no. COST/202/2006. The work-station cluster consisting of forty AMD Dual Core Opteron CPUs, on which the simulations were carried out, was purchased within the latter grant. The international co-operation, in turn, was co-financed by the governments of France and Poland within the programme POLONIUM.

References

[1] Biborski A, Zosiak L, Kozubski R, Pierron-Bohnes V. Lattice gas decomposition model for vacancy formation correlated with B2 atomic ordering in intermetallics. Intermetallics 2009;17:46–55.
[2] Schaefer H-E, Frenner K, Würschum R. High-temperature atomic defect properties and diffusion processes in intermetallic compounds. Intermetallics 1999;7:277–87.
[3] Kozubski R, Kmieć D, Partyka E, Danielewski M. "Order–order" kinetics in $Ni_{50.5}$ $Al_{49.5}$ single crystal. Intermetallics 2003;11:897–905.
[4] Oramus P, Kozubski R, Pierron-Bohnes V, Cadeville MC, Pfeiler W. Monte Carlo computer simulation of "order–order" kinetics in $L1_2$ – ordered Ni_3Al binary system. Phys Rev B 2001;63:174109/1–14.
[5] Schapink FW. The distribution of vacancies in ordered alloys of CsCl-type. Scr Metall 1969;3:113–6.
[6] Biborski A, Zosiak L, Kozubski R, Pierron-Bohnes V. Lattice-gas-decomposition model for vacancy formation correlated with B2 atomic ordering in intermetallics. In: Palm M, Bewlay BP, Takeyama M, Wiezorek JMK, He Y-H, editors. Advanced intermetallic-based alloys for extreme environment and energy applications. Mater. Res. Soc. Symp. Proc., vol. 1128; 2009. Warrendale, PA. 1128-U09-02.
[7] Binder K, Lebowitz JL, Phani MK, Kalos MH. Monte Carlo study of the phase diagrams of binary alloys with face centered cubic lattice structure. Acta Metall 1981;29:1655–66.
[8] Kofke DA, Glandt ED. Monte Carlo simulation of multicomponent equilibria in a semigrand canonical ensemble. Mol Phys 1988;64:1105–313.
[9] Dünweg B, Landau DP. Phase diagram and critical behaviour of the Si-Ge unmixing transition: a Monte Carlo study of a model with elastic degrees of freedom. Phys Rev B 1993;48:14182–97.
[10] Pareige C, Soisson F, Martin G, Blavette D. Ordering and phase separation in Ni–Cr–Al: Monte Carlo simulations vs three-dimensional atom probe. Acta Mater 1999;47:1889–99.
[11] Tavazza F, Landau DP, Adler J. Phase diagram and structural properties for a compressible Ising ferromagnet at costant volume. Phys Rev B 2004;70:184103/1–11.
[12] Cannavacciuolo L, Landau DP. Critical behaviour of the three-dimensional compressible Ising antiferromagnet at constant volume: a Monte Carlo study. Phys Rev B 2005;71:134104/1–134104/7.
[13] de Miguel E, del Rio EM, Telo da Gama MM. Liquid–liquid phase equilibria of symmetrical mixtures by simulation in the semigrand canonical ensemble. J Chem Phys 1995;103:6188–96.
[14] Lim SH, Murch GE, Oates WA. Thermodynamic properties of ternary alloys from Monte Carlo simulations. J Phys Chem Solids 1989;50:1251–9.
[15] Lim SH, Murch GE, Oates WA. Equilibrium vacancy voncetrations in non-stoichiometric B2 compounds by Monte Carlo simulations. J Phys Chem Solids 1992;53:181–7.
[16] Mishin Y, Mehl MJ, Papaconstantopoulos A. Embedded-atom potential for B2-NiAl. Phys Rev B 2002;65:224114/1–14.
[17] Kogachi M, Haraguchi T. Point defects in B2-type intermetallic compound. Mater Sci Eng A 2001;312:189–95.
[18] Breuer J, Sommer F, Mittemeijer EJ. Thermodynamics of constitutional and thermal point defects in B2 $Ni_{1-x}Al_x$. Philos Mag A 2002;82.
[19] Lozovoi AY, Mishin Y. Point defects in NiAl: the effect of lattice vibrations. Phys Rev B 2003;68:184113.
[20] Atanasov I, Hou M. Equilibrium ordering properties of Au–Pd alloys and nanoalloy. Surface Science 2009;603:2639–51.
[21] R. Sot, private communication.
[22] Nogueira RN, Schön CG. Embedded atom study of the interaction between point defect in iron aluminides: triple defects. Intermetallics 2005;13:1245–54.
[23] Aranovich GL, Erickson JS, Donohue MD. Lattice gas 2D/3D equilibria: chemical potentials and adsorption isotherms with critical points. J Chem Phys 2004;120:5208–16.